Tribology International 171 (2022) 107509

Contents lists available at ScienceDirect

Tribology International

journal homepage: www.elsevier.com/locate/triboint

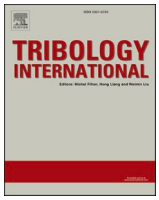

# A 2D dual-scale method to address contact problems

Mohammad Aramfard [a], Francisco Pérez-Ràfols [a], Lucia Nicola [a,b,*]

[a] Department of Industrial Engineering, University of Padova, I-35131 Padua, Italy
[b] Department of Materials Engineering, Delft University of Technology, 2628 CD Delft, The Netherlands

ARTICLE INFO

*Keywords:*
Multiscale modeling
Contact mechanics
Indentation
Friction

ABSTRACT

A seamless 2D dual-scale computational scheme is developed to study contact problems. The model consists of an atomistic domain close to the contact, coupled with an elastic continuum domain away from the contact. The atomistic formulation provides a description of the contact interaction through interatomic potentials and permits to capture atomic wear and defect formation in the contact region. The fields in the continuum domain are calculated by an efficient FFT-based Green's function method. The novel scheme is validated against full atomistic simulations and applied to study the effect of adhesion on the scratching of a rough copper surface by a rigid smooth spherical tip.

## 1. Introduction

Although the field of contact mechanics is more than a century old, it is still a subject of interest and importance [1–3]. It gained new attention with the development of MEMS, where surfaces of moving parts can undergo significant friction and wear, due to the increased surface-to-volume ratio of the components and the inevitable roughness and adhesion that occur at the nano-scale [4,5]. Surface roughness and adhesion are found to play a dominant role also in macro-scale applications involving contact, [6,7]. Real surfaces have self-affine roughness with wavelength spanning over various decades of length scale, including the nanometer scale. It has been shown that all these scales must be taken into account to capture accurately the contact response [8–10].

Different numerical methods have been developed to study the contact deformation of elastic solids with self-affine rough surfaces [11]. Boundary element methods, especially the ones relying on FFT have been found to be the most computational-efficient, outperforming the finite element method [12–14]. These techniques allow one to mesh the surfaces with a very high density of discretization points, thus spanning all wavelengths required. First contact occurs only at the tips of nano- and micro-scale scale asperities, which must sustain loads that give rise to very high local contact pressure. The pressure exceeds significantly the yield point of the material and is often responsible for non-linear behavior. This is why we deem important to model the contact regions not only elastically but also by considering possible non-linearities, including atomic wear and dislocation nucleation and glide. The most accurate way of modeling such non-linearities is the use of atomistic simulations. An important asset of atomistic simulations is also that they describe contact interactions accurately through interatomic potentials, and naturally include adhesion between surfaces, when present [15].

Considering only the nano-scale is not sufficient to tackle contact between micro- or macro-scale bodies, because what occurs at the nano-scale does not scale up, and treating large domains atomistically is either unfeasible or very time consuming. To overcome the computational burden of atomistic simulations, time efficient dual-scale modeling techniques have been proposed, where an atomistic domain has been coupled to a continuum domain. The most successful have been the Quasi Continuum QC method [16], the Coupling of Length Scales (CLS) method [17], the Finite Element combined with Atomistic modelling (FEAt) [18] and the Coupled Atomistic and Discrete Dislocation plasticity method CADD [19]. These techniques could succesfully address problems like incipient plasticity under indentation [20] and crack propagation [21]. In all these dual-scale methods the coupling occurs between an atomistic domain and an elastic continuum, modeled by means of the finite element method. CADD, which is similar to CLS and FEAt, has the added value to include discrete dislocations in the continuum region, which can thus deform also through dislocation plasticity.

For application to contact problems it is computationally more efficient to rely on boundary element methods to treat the continuum domain, which is sufficiently far away from the contact to have smooth fields that do not require a finer discretization than what is provided at the interface. Pastewka *et al.* [22] proposed a method to approximate the

* Corresponding author at: Department of Industrial Engineering, University of Padova, I-35131 Padua, Italy.
*E-mail address:* lucia.nicola@unipd.it (L. Nicola).

https://doi.org/10.1016/j.triboint.2022.107509
Received 7 January 2022; Received in revised form 15 February 2022; Accepted 24 February 2022
Available online 4 March 2022
0301-679X/© 2022 The Authors. Published by Elsevier Ltd. This is an open access article under the CC BY license (http://creativecommons.org/licenses/by/4.0/).

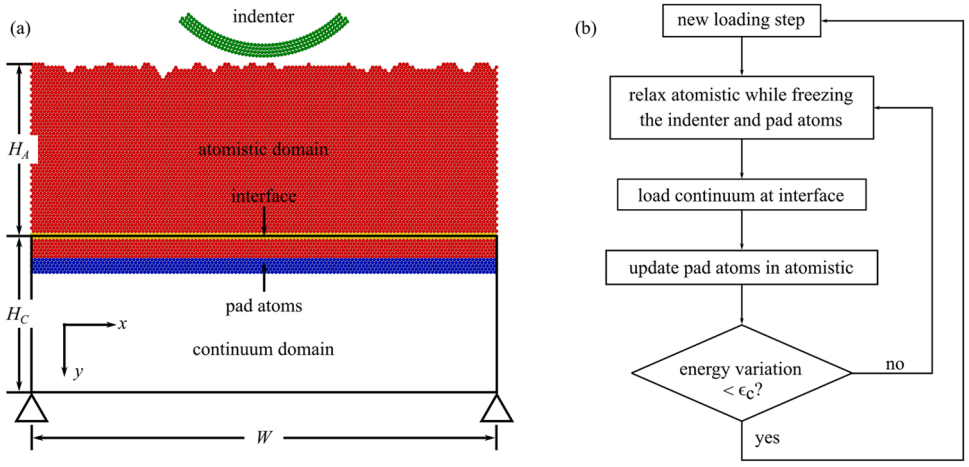


**Fig. 1.** (a) Schematic representation of the dual-scale structure. Indenter atoms are green, crystal atoms red, interface atoms yellow, and pad atoms blue. (b) Flowchart of the dual-scale scheme. (For interpretation of the references to colour in this figure legend, the reader is referred to the web version of this article.)

substrate up to harmonic order using a Green's function formulation. Their seamless method is efficient at the interface of the atomistic and continuum domains and is not affected by ghost forces, a problem that was encountered in the models coupling MD and FEA [23]. A small drawback of the method is that it is crystal orientation specific and thus not very versatile in its use, since the Green's functions need to be derived for the specific crystal lattice.

Here, we propose a more flexible method where the atomistic domain is linked through pad atoms to a generic linear elastic isotropic domain, described through Green's functions. The orientation of the atomistic crystal is thus transferred to the continuum domain only through its elastic constants, and therefore the response is slightly less accurate than the one obtained by [22]. Loading of the continuum domain, whose surface is flat, occurs through the tractions imposed by the atomistic domain. When computing the equilibrium static solution, energy minimization is enforced explicitly on the atomistic domain only, to reduce the computational burden, while guaranteed everywhere by the concurrent coupling.

To validate the dual-scale model we perform two-dimensional simulations of indentation and shallow scratching of a thin copper layer by means of a cylindrical indenter and compare the results with those of full-atomistic simulations for the same problem. The analysis is performed on a section of the film (the x-y plane in Fig. 1) considering plane-strain conditions: the displacements of the atoms in the out-of-plane direction $z$ are set to zero at each time step of the simulation. After validation, we perform simulations with the dual-scale model to investigate what are the qualitative differences between scratching a rough metal crystal with an adhesive and a non adhesive indenter for copper films with various thickness. Two-dimensional and quasi-three-dimensional simulations were often performed at the advent of molecular dynamics simulations to limit the number of atoms in the model due to limitations in the computational facilities. Nowadays, they are still carried out for various problems, including the study of interfaces, twins and grain boundaries, and their interaction with dislocations [24–27], crack nucleation [28], phase transitions [29], nanoindentation [30], and mostly in the framework of multi-scale modeling [19,31,32].

This article is organized as follows: Section 2 explains the methodology, provides details on both domains and on the coupling between them. Validation through comparison to full size atomistic simulations for indentation and light scratching of smooth and rough copper surfaces is presented in Section 3. The effect of increasing height of the body by increasing the height of the continuum domain is studied in Section 4 for the light scratching of rough copper crystals by means of a rigid and smooth spherical indenter.

## 2. Methodology

A 2D dual-scale single crystal of width $W$ is constructed with the top part, of height $H_A$, described by an atomistic domain and the bottom part, of height $H_C$, described by a continuum domain as shown in Fig. 1 (a). In this way, the material is modeled atomistically close to the contact, where non-linear behavior is expected to prevail, and as a linear elastic continuum elsewhere. The continuum solution is obtained using a Green's function formulation, which is described in Section 2.2. The atomistic and continuum domains are coupled concurrently through pad atoms shared by both domains. The pad atoms comprise five layers of atoms so that the height of the region exceeds the cut off distance of the force field.

The deformation is transferred from the continuum to the atomistic domain by means of pad atoms which are shared by the two domains: the pad atoms impose displacement boundary conditions to the bottom of the atomistic domain after their positions are updated in response to the deformation of the continuum domain.

The algorithm used to couple the continuum and atomistic domains is summarized in Fig. 1 (b) for the case study of the indentation of a single crystal. Note that the scheme presented here has sufficient flexibility to admit any type of quasi-static loading that can be applied in a generic atomistic simulation. Here, an incremental load is applied to the surface of the crystal by displacing normally the indenter. First, as in a typical molecular statics simulation, the position of the atoms in the atomistic domain is updated by minimizing the potential energy while keeping the pad atoms fixed (the pad atoms are represented in blue in Fig. 1). Then, the stress at the bottom of the atomistic domain is computed at the atoms that in Fig. 1 are represented in yellow: the atoms where the stress is computed are taken to be at a distance from the pad atoms of the same order as the force field cut-off distance. This is to avoid spurious effects caused by the presence of the fixed pad atoms. The stresses are then interpolated to the grid-points that discretize the continuum domain and used to impose traction boundary conditions to the continuum. The displacement caused by the imposed tractions on the continuum is computed using the Green's function method. At this point also the position of the pad atoms is updated as if they moved by being rigidly linked with the deforming continuum domain. The displacement of the pad atoms is then used to load once more the atomistic domain, while the indenter is still frozen. The energy is again minimized in the atomistic domain, new equilibrium positions are found for the atoms and the stress is again computed at the interface to load once more the continuum domain. Such iterative procedure continues until the variation in energy of the atomistic domain over the last three iterations, computed using a finite difference backward scheme, is smaller than a

small quantity that we take to be $\epsilon_c = 10^{-4}$ eV. Then the iteration is terminated and the next incremental indentation step is initiated. Here, the energy is explicitely minimized in the atomistic domain only, instead of in both domains as done in other work (*e.g.* Shilkrot *et al.* [19]), with the aim of reducing the computational time.

Convergence to equilibrium is easier reached when the height of the continuum domain is small, because its deformation induces small displacements of the pad atoms. However, the model becomes really useful only when the continuum domain is large, *e.g.* when $H_C$ is at least one order of magnitude larger than $H_A$. Convergence is improved for large values of $H_C$ by limiting the variation of the traction vector acting on the continuum domain from an iteration to the next. This is done by introducing a virtual spring between the current and previous traction vectors, similarly to the Nudged Elastic Band (NEB) method explained in [33].

### 2.1. Atomistic domain

The interaction between the atoms in the crystal is described using the Embedded Atom Method (EAM) [34] many-body interatomic potential, parametrized by Mishin *et al.* [35] for copper. The indenter is modeled as a rigid hollow and smooth cylinder. The reason for selecting a smooth spherical rigid indenter instead of a real crystal is that a spherical shape carved in a nano-scale crystal is atomically stepped. The steps in the surface would play a dominant role in the contact and scratching behavior, and affect significantly adhesion. Here we prefer to focus on how a rough surface deforms when the indenter is atomically smooth and does not deform.

To isolate the effect of adhesion, we take the indenter to be either in adhesive or in non adhesive contact with the crystal. The adhesive interaction between the rigid indenter and the crystal is modeled through the same EAM force field used for the crystal. For the non adhesive interaction, we select instead the Morse potential, because the adhesive contribution of the field can be easily removed from pair-wise potentials. Only the portion of the energy function which results in repulsive force is used by setting the cut-off distance equal to the equilibrium distance ($r_0$). Following the work by Lincoln *et al.* [36] the value of the equilibrium distance is taken to be $r_0 = 2.8985$ $\mathring{A}$, and the values for the cohesion energy and elastic energy to be $D_0 = 0.3282$ eV and $\alpha = 1.3123$ $\mathring{A}^{-1}$, respectively.

To describe the copper crystal in two dimensions, we have considered a single atomic plane, namely the (111) plane, to coincide with the *x*-*y* plane of analysis. The displacements of the atoms as well as the forces acting on them in *z*-direction are set to zero at each time step of the simulation (see https://docs.lammps.org/Howto_2d.html). This entails that the FCC crystal is not explicitly described in the *z*-direction, i.e. neither the spacing between atomic planes nor the interactions between atoms in *z*-direction enter in the picture, but the behavior is inferred through the plane strain analysis. For a more realistic analysis of the behavior of an FCC crystal, many authors consider a quasi-3D description of the crystal, where at least three layers of atoms repeat periodically. In the framework of a dual-scale model, where the atomistic domain is coupled with a two-dimensional continuum, considering more than one atomic layer is however not possible. The same 2D approach was used by [37,23,38]. The (111) plane is selected to be in the plane of analysis, as done in similar studies [19,39,31], because it is the plane of easy glide for edge dislocations in FCC crystals. The dislocations that can be observed in these simulations have Burgers vector $a < 11\bar{2}0 >$

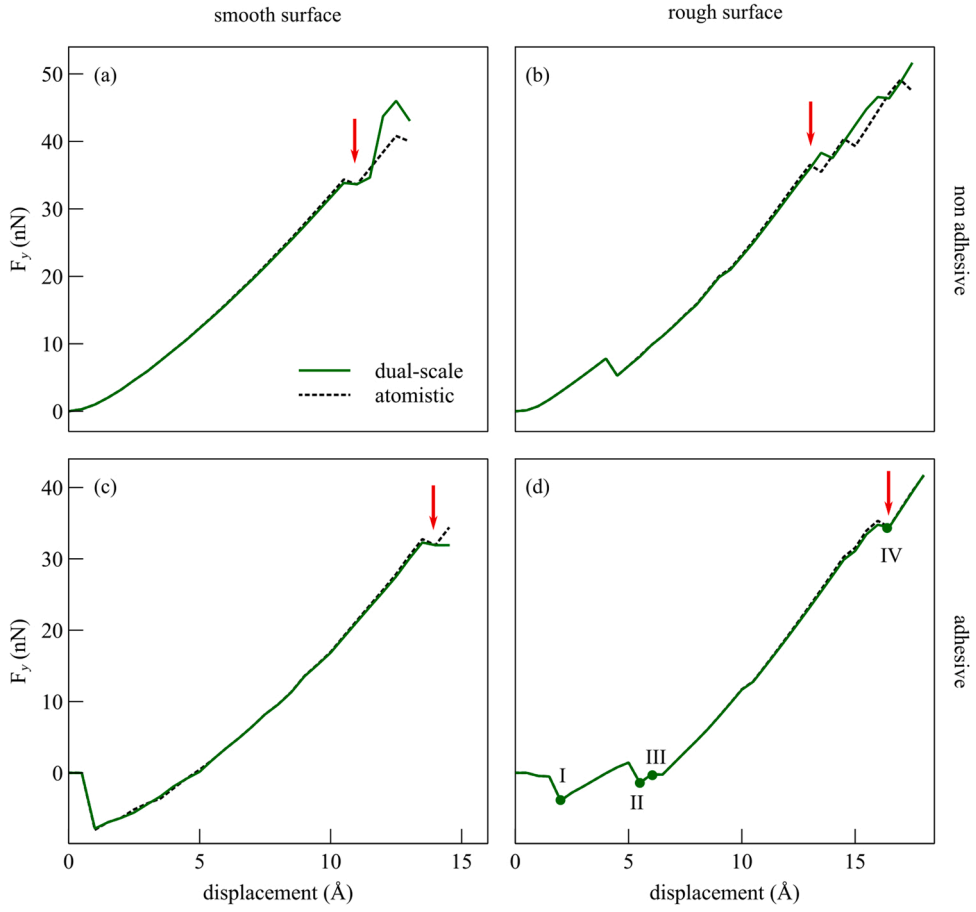


**Fig. 2.** Force vs. displacement curves resulting from indentation of (a) a non adhesive smooth, (b) a non adhesive rough, (c) an adhesive smooth and (d) an adhesive rough surface. Red arrows show the points where a dislocation reaches the interface between domains and the dual-scale model is no longer valid.

contained in the (111) plane. The lattice parameter is $a = 2.46$ Å. The dimensions of the crystal are $H_A = 10$ nm and $W = 31$ nm, corresponding to 7784 atoms. Periodic boundary conditions are imposed in $x$-direction.

The indenter is taken to be rigid and hollow with outer radius of 8 nm. The top surface of the crystal is taken to be either flat or rough. The rough surface is constructed as self-affine with a Gaussian height distribution. A rough profile is first generated with rms-height $s_q = 3$ Å, Hurst exponent $H = 0.5$ and wavelength cut-off $q_r = 100$. To minimize the energy of the surface atoms, a relaxation run is performed using a NPT Nosé-Hoover thermostat [40,41] at 800$K$ for 100$ps$ at zero pressure in the periodic direction. The temperature is brought to 1$K$ with a quenching rate of 8 K/ps and relaxed using NPT at 1 K for 20 ps.

The Large-scale Atomistic/Molecular Massively Parallel Simulator (LAMMPS) is used to find the configuration with minimum potential energy of the crystal by means of the Fast Inertial Relaxation Engine (FIRE) [42] followed by the conjugate gradient method at 0 K. Stress is computed using the virial formulation [43].

### 2.2. Continuum domain

The continuum domain has the same periodic length as the atomistic domain and is taken to have various heights. The top surface, which corresponds to the interface with the atomistic domain, is initially flat and is discretized through grid-points spaced as the atoms. The bottom surface of the domain, although not explicitly modeled, is fixed. Periodic boundary conditions are implicitly imposed in $x$-direction.

A Green's function method is used to find the deformation for any given point $(x,y)$ in the domain. For that, the tractions applied at the nodes are Fourier transformed in $x$-direction. The displacements are then computed as a function of these tractions as

$$\begin{bmatrix} u_x^{\mathrm{I}}(q,y) \\ u_y^{\mathrm{I}}(q,y) \end{bmatrix} = \begin{bmatrix} G_{xx}(q,y) & G_{xy}(q,y) \\ G_{yx}(q,y) & G_{yy}(q,y) \end{bmatrix} \begin{bmatrix} T_x^{\mathrm{I}}(q,y) \\ T_y^{\mathrm{I}}(q,y) \end{bmatrix} \tag{1}$$

where $q$ is the wavevector, $T_i^I$ are the tractions, $u^I$ are the displacement and $G_{ij}$ are the Green's functions, given in Appendix. Finally, inverse Fourier transforms are used again to retrieve the displacements of the points $(x,y)$ in the real domain. The interested reader is directed to Nyqvist *et al.* [45] or Venugopalan *et al.* [46] for a detailed derivation of (1), while here only a short description of the main steps will be given. The equations for linear elasticity are transformed to Fourier space in $x$-direction while the boundary conditions are applied in real space. This results in a set of equations that only contains derivatives with respect to $y$ that can be solved analytically. Note that, since the Green's functions are an analytical solution of the equations of elasticity, no iteration is required within the continuum domain.

The continuum domain is here treated as an elastic and isotropic material. To select elastic constants that would minimize mismatch between continuum and atomistic domains, a tensile test was performed on the atomistic crystal, by loading in the same orientation used subsequently for indentation. This allowed us to measure the average contraction of the crystal in the elastic regime, and determine the elastic modulus and the Poisson's ratio to be used for the continuum: E = 181 GPa and $\nu = 0.32$.

## 3. Validation

### 3.1. Indentation

The dual-scale scheme is validated against full atomistic simulations for four test cases: two crystals with smooth and rough surface are indented with and without adhesion. The total height of the crystal is $H_{TOT} = 20$ nm. In the dual-scale model the height of the atomistic domain and of the continuum domain are $H_A = 10$ nm and $H_C = 10$ nm,

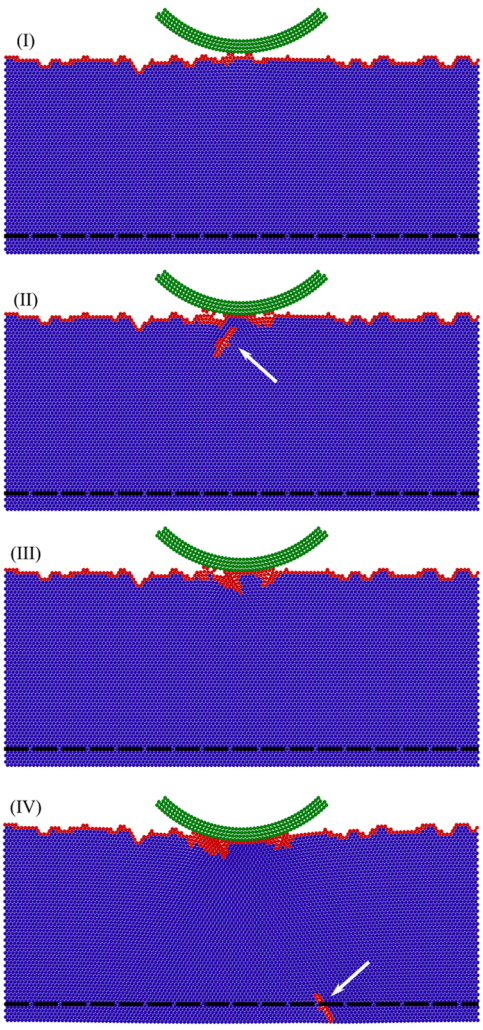


**Fig. 3.** CNA of the atomistic domain in adhesive indentation of rough surface shown in Fig. 3 (d): (I) Initial contact, (II) dislocation nucleation under the indenter, (III) dislocation is absorbed back to the surface, (IV) dislocation nucleates and migrates to the interface. (For interpretation of the references to colour in this figure legend, the reader is referred to the web version of this article.)

respectively. The loading step is set to be $u_y = 0.5$ Å. The increase in normal force during indentation is shown in Fig. 2: on the left column the curves correspond to indentation of the crystal with (a) non adhesive and (c) adhesive flat surface; on the right column the indentation of a crystal with (b) non adhesive and (d) adhesive rough surface. The non adhesive smooth surface shows the usual Hertzian response until a dislocation is nucleated at an indentation depth of approximately 11 Å. The nucleated dislocation immediately travels toward the middle of the crystal and, when it reaches it, there is the expected discrepancy between full atomistic and dual-scale results. The red arrow indicates the point when full atomistic and dual-scale stop matching. A similar curve, albeit with initial tensile response due to adhesion is observed for the smooth adhesive surface in Fig. 2 (c). When the crystal surface is rough, the curves are less smooth, but the agreement between the two models is still excellent until a dislocation reaches the interface between domains.

The Common neighbor analysis (CNA) [44] is performed on the atomistic domains to track the formation of defects during the simulations. Fig. 3 shows representative snapshots of the simulation of indentation of a rough adhesive surface in Fig. 2 (d), which is characterized by the roughest force-displacement curve. The salient points where the snapshots are taken are labeled in Fig. 2 (d) with roman

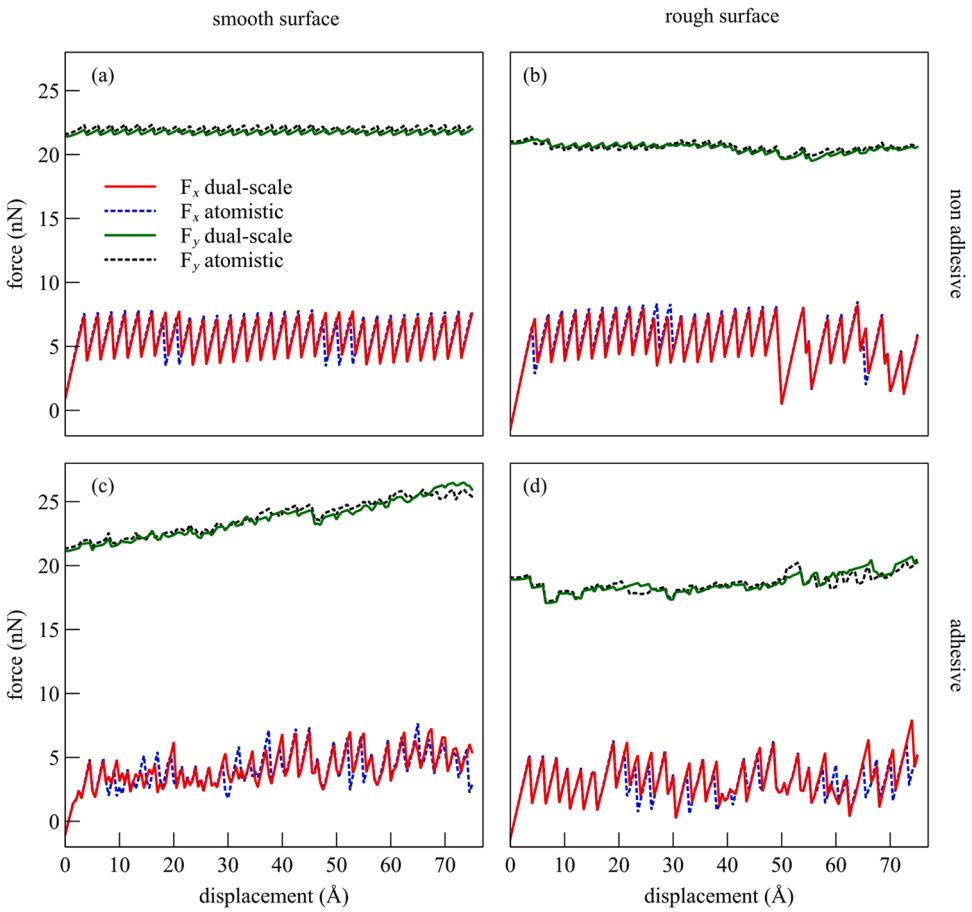


**Fig. 4.** Normal and tangential force vs. tangential displacement curves resulting from light scratching of (a) a smooth and (b) a rough surface without adhesion, and (c) a smooth and (d) a rough surface with adhesion.

numbers.

In Fig. 3, blue is used to color atoms that are still in their hexagonal configuration, while red indicates atoms that do not correspond to the hexagonal coordination and are therefore defects in the crystallographic structure. The indenter is shown in green and the dashed line shows the position of the interface. A white arrow is used to indicate dislocations. The first drop in the load-displacement curve, which is indicated by (I), and denotes a sudden increase in tensile contact pressure happens when the adhesive force between the indenter and the surface snap into contact. The second drop in the curve, indicated by (II), is caused by the nucleation of a dislocation under the indenter. The dislocation does not travel far away but is absorbed back into the surface in a subsequent loading step (III). It is noteworthy, that nucleation of defects is properly captured by the dual-scale method and no deviation is observed from the behavior of the full atomistic simulation unless the dislocation reaches the interface. This is what happens at snapshot (IV), where a different dislocation reached the continuum domain.

### 3.2. Light scratching

To further validate the dual-scale model, simulations are performed for a light scratching (the imposed normal load is small) of smooth and rough surfaces. The indenter is first displaced normally to a depth $\Delta y = 11\ \AA$ and $\Delta y = 12.5\ \AA$ for smooth and rough surfaces, respectively, then tangentially of $\Delta x = 75\ \AA$. $\Delta y$ was chosen such that no dislocation reaches the interface before scratching starts, to make sure that we are still in the regime where the dual-scale method provides the correct response. Normal and tangential forces as a function of the tangential displacement of the tip are presented for a smooth and a rough surface with and without adhesion in Fig. 4. The best agreement with full atomistic simulation is found for the scratching of the non adhesive surfaces in Fig. 4 (a) and (b), while the presence of adhesion leads to local tiny differences in the curves. Even though the roughness is constructed identical, loading of the two systems leads to small discrepancies in atomic locations, which are magnified during loading. The source of discrepancy between full atomistic and dual-scale simulations is that the dual-scale method approximates the continuum as if it were linear elastic and isotropic. This approximation induces an error, because upon loading the deformation of the isotropic continuum, with fitted Poisson's ratio, is slightly different than that of an anisotropic crystal. This small difference affects negligibly the simulations where the interaction is non adhesive, but is enhanced when the scratching is done on an adhesive surface, even more so if it is rough. The reason is that the surface atoms, that have already a smaller coordination number than those in the crystal, can be more easily displaced when also subjected to an attractive force. The attractive force can induce an instable movement of the surface atoms that might attach to the indenter or displace tangentially. This is why tiny initial differences obtained during indentation are amplified during scratching.

The lateral force experienced by the tip probing the flat non adhesive surface displays the typical stick-slip behavior observed in AFM friction tests, because the normal load is very small. It is noteworthy, that the lateral force for adhesive surfaces is, perhaps surprisingly, on average smaller than for non adhesive surfaces. The reason is that it is easier for the tip to dislodge and wear away atoms that, owing to adhesion, tend to adhere to the tip and do not occupy the typical low-energy atomic position in the lattice of the copper substrate. Indeed, when the surface is adhesive, the stick-slip features are characterized by a smaller

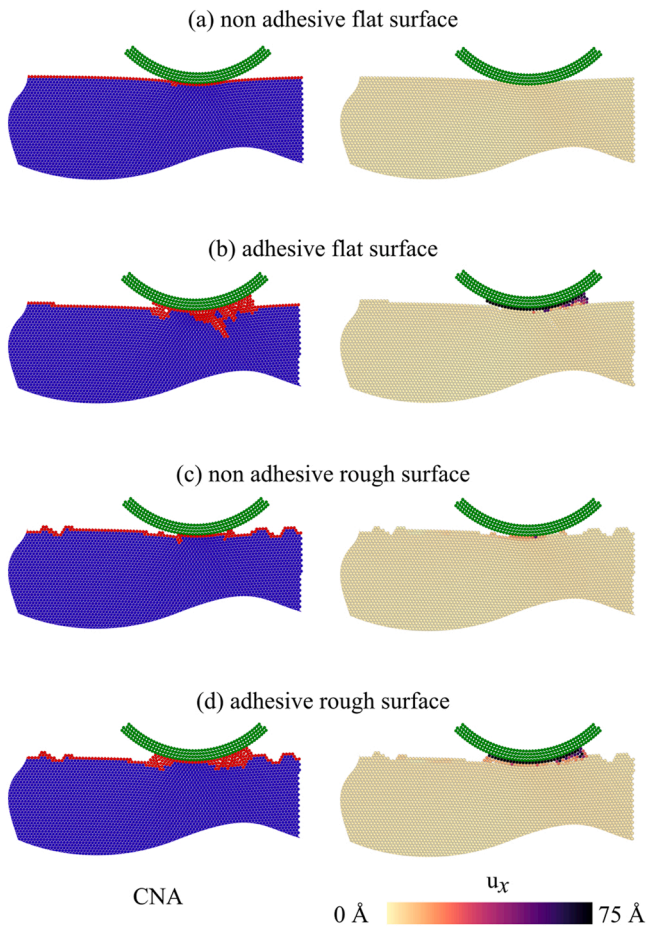


**Fig. 5.** CNA and atomic displacement distribution for the light scratching of the crystals in Fig. 4 with (a) non adhesive flat, (b) adhesive flat (c) non adhesive rough, and (d) adhesive rough surface. Blue atoms have hexagonal coordination, red atoms have other coordination. The rigid indenter is shown in green. (For interpretation of the references to colour in this figure legend, the reader is referred to the web version of this article.)

amplitude, and by a less regular pattern than when surfaces are non adhesive, just because the energy required to drag away the contacting atoms is smaller. This can be seen in the final configurations of the atomistic domain provided in Fig. 5, which are colored according to the CNA on the left hand side and according to the lateral displacement of the atoms on the right hand side.

For this very light scratching it appears that the atoms engaged by the tip and that displace under its action are only very few and localized below the tip. Fig. 5 show also that in the case of adhesive scratching the lateral force increases on average, owing to atomic wear and material piling up in front of the contact. Rough surfaces present similar features to smooth surfaces, with the difference that the pattern followed by the lateral force is less regular, since it is affected by irregularities in the surface topography. The material worn from the surface can be hosted by the nano-valleys in front of the tip.

The supplementary material contains movies of the simulation of scratching of a non adhesive rough surface (S1) and, of an adhesive smooth (S2) and adhesive rough surface (S3).

## 4. Height of the crystal

The dual-scale method is used to study the effect of crystal size on adhesive and non adhesive scratching of rough surfaces. The atomistic domain is kept unchanged while the height of the continuum domain is increased from 10 nm to 1 μm. The scratching length is chosen to be 70 $\AA$ after the first slip event, which occurs at smaller displacements for thinner crystals. The reason for the difference is that thicker crystals undergo approximately the same elastic shear strain as the thinner ones before slip occurs, which corresponds to a larger tangential displacement of the top surface. The tangential and normal forces as a function of tangential displacements are shown in Fig. 6 (a) and (b), and Fig. 6 (e) and (f) for crystals of various heights. The curves for small crystal heights present various fluctuations around a changing mean that are caused by the typical stick slip behavior of the AFM tip. As expected, the amplitude of oscillation of the stick-slip pattern in the lateral force increases with increasing normal force, *i.e.*, decreasing crystal height, for both adhesive and non adhesive surfaces. To better distinguish the curves for different crystal heights, the same curves shown in Fig. 6 (a) and (b) are presented once more in Fig. 6 (c) and (d) after smoothening through a weighted moving average of bin size 7. The elastic shearing is clearly distinguishable in Figs. 6 (a, b, c, d) since it corresponds to the linear force-displacement curve at small loading. It is noteworthy that the thickest films are herein included mostly to show that the model can address larger domains, but their scratching behavior can be compared with that of the thinner layers only after the initial shearing of the crystal, when slip starts, i.e. at large tangential diplacement. In these simulations the indenter is displaced vertically of the same distance $\Delta y = 12.5\,\AA$ from the surface for all cases, thus the normal force the indenter exerts on the crystal decreases with increasing height, as can be seen in Fig. 6 (e) and (f).

The main difference between the scratching response obtained for adhesive and non adhesive interfaces is that the curves for non adhesive surfaces are sensitive to the height of the crystal, with thicker crystals giving rise to a smaller lateral force than the thinner ones. This dependence on height of the non adhesive crystals is attributed to the difference in the normal force exerted by the indenter on the surfaces: the thinner the crystals the larger the normal force, the larger the resistance to scratching. On the contrary, the average lateral force on adhesive rough surfaces appears independent of crystal height, indicating that for the simulation parameters selected, it is adhesion that controls the scratching response. An additional difference between curves of lateral force for adhesive and non adhesive surfaces is that the first are very jagged and their shape bears no resemblance with the pristine roughness of the surface, while the shape of the second can be correlated to the roughness profile of the surface. It is noteworthy in this respect that, despite the surface profiles before indentation and scratching are all the same, the profile changes during indentation in a way that depends on crystal height. This is why, although resembling the surface profiles before scratching, the curves are not all having the same shape. In the case of non adhesive surfaces, the scratching behavior is controlled mostly by the geometry of the crystal, i.e., its roughness and its height. This is a case where it is critical to model the full height of the body, if one is interested in the details of how the lateral force changes. The response does not scale with crystal height due to the non-linear behavior of the atoms, during both indentation and scratching. In the case of adhesive contacts the results have instead lead to conclude that adhesion, for the simulation parameters selected, fully controls the scratching response and that the crystal geometry, including both its thickness and roughness, play a negligible role.

As an additional proof that the non adhesive curves are correlated to roughness while the non adhesive are not, a new crystal is constructed of height $H_C = 100$ nm but with a different rough surface profile (that we will label as s2) than the one characterized by the light blue curve in Fig. 6 (c) and (d), which we will label in the following as s1.

The tangential forces obtained by scratching the new crystal with adhesive and non adhesive interaction is contrasted in Fig. 7 with the response obtained with the previous roughness s1. The two curves for non adhesive surfaces are markedly different and indicate that the surface profile s2 is initially flatter than s1 and that after a rather pronounced valley the profile becomes again rather flat. This features cannot be observed when adhesion is active, because the surfaces

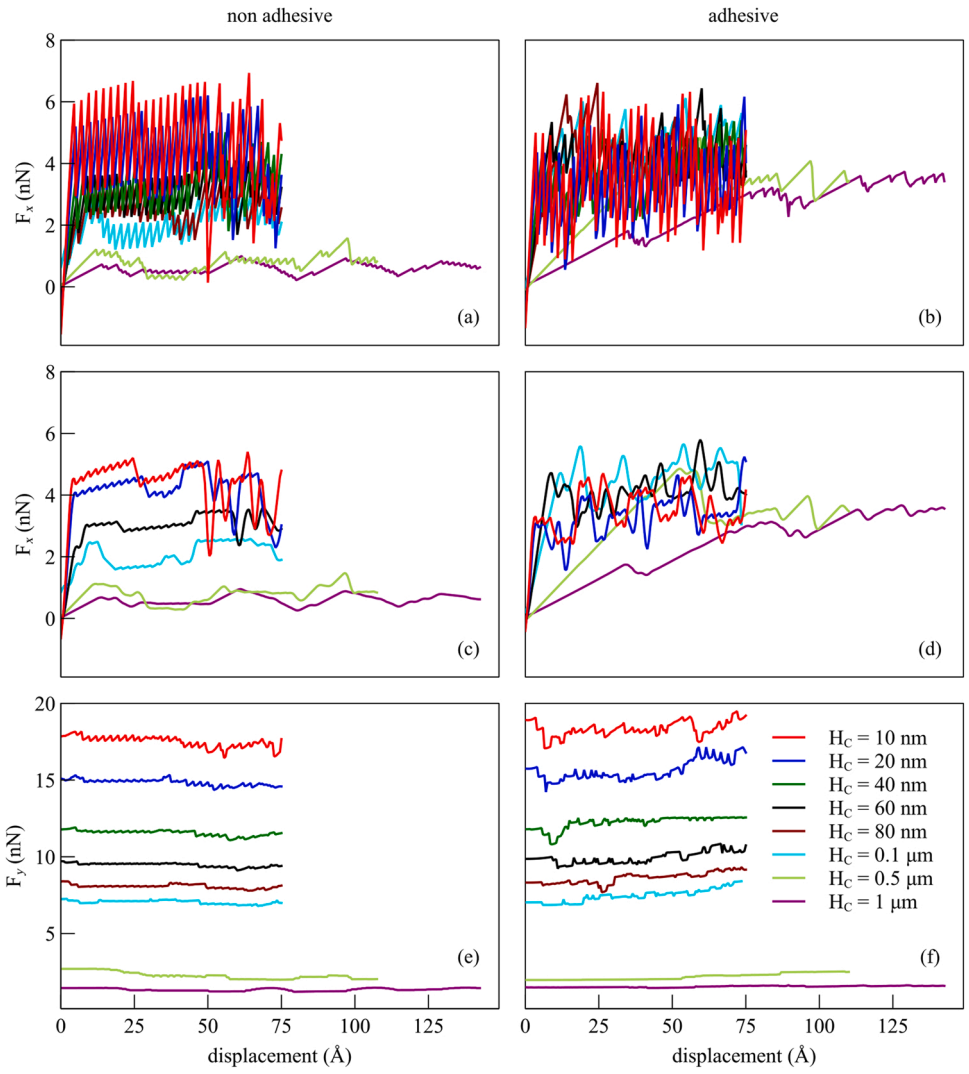


**Fig. 6.** Scratching of crystals with rough surface and various heights: tangential force calculated while the tip is displaced tangentially on a (a) non adhesive and (b) adhesive rough surface. Moving average of the tangential force during tangential displacement of the tip on a (c) non adhesive and (d) adhesive surface. Normal force vs. tangential displacement of (e) non adhesive and (f) adhesive contacts.

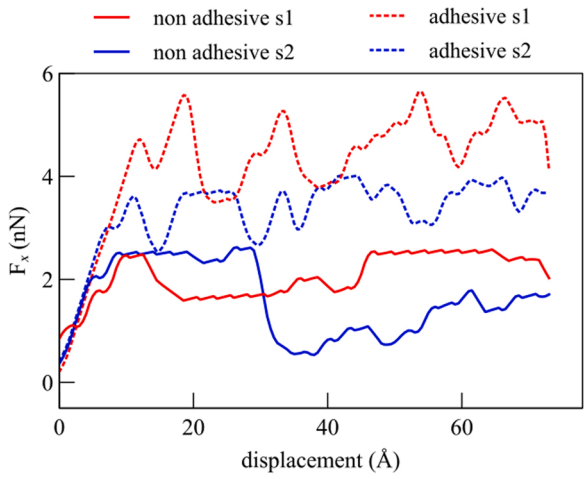


**Fig. 7.** Tangential force calculated while the tip is displaced tangentially on adhesive and non adhesive surfaces s1 and s2.

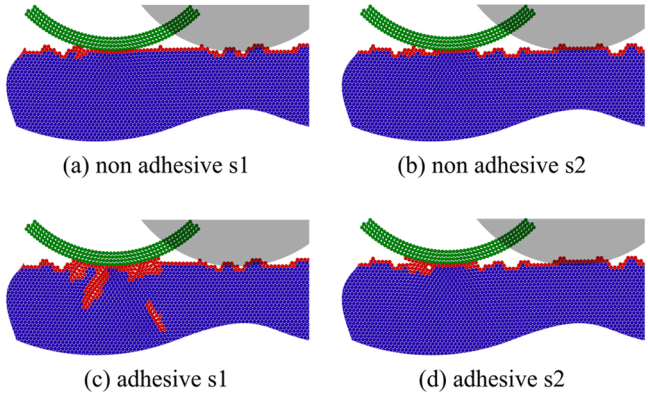


**Fig. 8.** CNA after indentation, but before scratching, of the crystals in Fig. 7. Blue atoms have hexagonal coordination, red atoms have other coordination. The rigid indenter is shown in green while the grey shade shows the final position of the indenter. (For interpretation of the references to colour in this figure legend, the reader is referred to the web version of this article.)

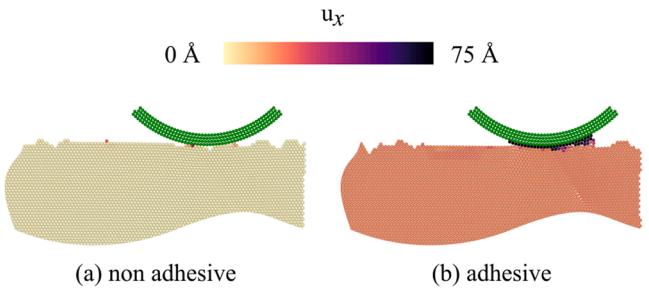


**Fig. 9.** Atomic displacement distribution for the light scratching of the crystals in Fig. 6 with (a) non adhesive and (b) adhesive rough surface with $H_C = 100nm$.

changes much more locally, with various atoms being dislodged and displaced to fill the valleys in front of the tip. The atomic structure of the films after indentation but before scratching are represented in Fig. 8. The gray shape indicates the end position of the indenter after scratching, so that the reader can see its complete path.

When contrasting the average lateral forces for adhesive and non adhesive surfaces it appears evident that when the normal load is smaller the lateral force is larger for the adhesive surfaces (contrast the light blue curves in Fig. 6) while the difference disappears at smaller normal load. This is because the indenter engages so little with the non adhesive surface that the few atoms on its path are easily displaced from the surface and moved to a nano-valley. The displaced atoms can be seen in Fig. 9, where it is also possible to see that in the adhesive thicker substrate many more atoms have moved with the tip.

The dual-scale model is approximately twice as fast for the 1 μm layer compared to the full atomistic simulation. The gain in speed increases significantly with the height of the crystal considered given that the atomistic simulation computational time scales with height with a larger coefficient than the dual-scale model. Notice that time comparison is not straightforward in that simulation time depends rather strongly on the specific system one models: if there is formation of more defects in the atomistic region, both simulations become slower of a quantity that does not scale with height and is not identical in the two methods. Also, the dual-scale model has the advantage to be more resource effective, because one does not need to store the data of all the atoms in the crystal.

In the supplementary material, the movie labeled as S4 shows the simulation of the scratching of the adhesive rough surface with $H_C$ = 100 nm. In this simulation two dislocations nucleate under the indenter when it is displaced normally, but when the indenter starts scratching and the compressive load on the dislocations is partially relieved, they are absorbed back to the surface.

## 5. Conclusions

A 2D dual-scale method is presented to concurrently exploit Green's function based BEM and atomistic simulations to address contact mechanics problems. An atomistic domain describes the near contact area and a linear elastic continuum domain the rest of the body. In an iterative procedure that leads to equilibrium, the continuum domain is loaded by the tractions at the bottom of the atomistic domain, while the atomistic domain is loaded at its bottom by the displacement of pad atoms, that lay inside the continuum domain. To increase convergence speed to a minimum energy for the atomistic domain, a spring is defined between the previous and current traction vector at the interface between domains, to ensure that the deformation of the continuum is limited. The dual-scale scheme presented here works for any two bodies in contact, provided the interatomic potential of each of the bodies and the interaction between them is given. Also, there are no limitations to extend the model in three dimensions, except for the additional computational burden.

The dual-scale scheme is here validated by comparison with atomistic simulations in the cases of indentation and scratching of copper crystals by means of a rigid smooth spherical indenter. The force-displacement response of the crystals matches the full atomistic simulations until dislocations reach the interface, and the method is no longer valid.

After validation, the dual-scale scheme is herein applied to model the light scratching of adhesive and non adhesive rough surfaces of crystals with various heights. The advantage of the dual-scale model is indeed that it allows one to increase the size of the continuum domain at low computational cost. The force-displacement curves obtained by scratching non adhesive rough surfaces are found to depend on crystal geometry, i.e., its height and roughness. This is at odds with what occurs when adhesion is considered: the force-displacement curves are independent of crystal geometry, for the simulation parameters selected in this work.

It is noteworthy that the simulations presented here are two-dimensional and as such have limitations on realism. The FCC crystal is modeled as a single layer of atoms and the dislocations are bound to be straight in the out-of-plane direction. Nevertheless, the simulations succeed in showing the agreement between the dual-scale model and the full-atomistic simulations and in providing evidence of the difference between the scratching response of adhesive and non adhesive rough crystals. It is expected that a three-dimensional analysis will not change these conclusions, but it would definitely lead to quantitatively different results. Three dimensional simulations would include full dislocation loops, and their interaction with other loops. This is expected to be of relevance when performing simulations to a larger indentation depth, where plasticity will have a leading role.

The model will be extended in future work to account for a continuum domain that can also deform plastically through dislocation dynamics. This will enable us to study contact deformation at larger indentation depth.

## Declaration of Competing Interest

The authors declare the following financial interests/personal relationships which may be considered as potential competing interests: Lucia Nicola reports financial support was provided by European Commission.

## Acknowledgement

This project has received funding from the European Research Council (ERC), Belgium under the European Union's Horizon 2020 research and innovation programme (grant agreement no. 681813).

## Appendix A. Green's functions

The Green's functions in (1) are given by

$$G_{xx} = (A_x + B_x qy)e^{qy} + (C_x + D_x qy)e^{-qy-qH_{GF}} \tag{A.1a}$$

$$G_{yy} = -i\left(A_y + kB_y + B_y qy\right)e^{qy} - -i\left(-C_y + kD_y - D_y qy\right)e^{-qy-qH} \tag{A.1b}$$

$$G_{xy}\left(A_y + B_y qy\right)e^{qy} + \left(C_y + D_y qy\right)e^{-qy-qH} \tag{A.1c}$$

$$G_{yx} = -i(A_x + KB_x + B_x qy)e^{qy} - i(-C_x + KD_x - D_x qy)e^{-qy-qH}, \tag{A.1d}$$

where

$$A_x = \left[-(k-1)k/(\mathrm{e}^{-2\mathrm{qh}}+1) + \mathrm{qh}(\mathrm{k}+1-2\mathrm{qh})\cosh(\mathrm{qh})^{-2}/2\right] \tag{A.2a}$$

$$B_x = \left[2k\tanh(qh)/(\mathrm{e}^{-2\mathrm{qh}}+1) + (\mathrm{k}-1+2\mathrm{qh})\cosh(\mathrm{qh})^{-1}/2\right] \tag{A.2b}$$

$$C_x = \left[(k-1)ke^{-qh} + qh(k+1+2qh)\cosh(qh)^{-1}\right]/(\mathrm{e}^{-2\mathrm{qh}}+1) \tag{A.2c}$$

$$D_x = \left[-2ke^{-qh}\tanh(qh) + (k-1+2qh)\cosh(qh)^{-1}\right]/(\mathrm{e}^{-2\mathrm{qh}}+1) \tag{A.2d}$$

$$A_y = i\left[(k+1)k\tanh(qh)/(\mathrm{e}^{-2\mathrm{qh}}+1) + \mathrm{qh}(\mathrm{k}+1-2\mathrm{qh})\cosh(\mathrm{qh})^{-2}/2\right] \tag{A.2e}$$

$$B_y = i\left[-2k/(\mathrm{e}^{-2\mathrm{qh}}+1) + (\mathrm{k}+1-2\mathrm{qh})\cosh(\mathrm{qh})^{-2}/2\right] \tag{A.2f}$$

$$C_y = i\left[-(k+1)ke^{-qH}\tanh(qh) - qh(k+1+2qh)\cosh(qh)^{-1}\right]/(\mathrm{e}^{-2\mathrm{qh}}+1) \tag{A.2g}$$

$$D_y = i\left[2ke^{-qh} + (k+1+2qh)\cosh(qh)^{-1}\right]/(\mathrm{e}^{-2\mathrm{qh}}+1) \tag{A.2h}$$

$$f = qG\left(4k - (4q^2h^2 + (4\nu-2)^2)\cosh(qh)^{-2}\right) \tag{A.2i}$$

## Appendix B. Supporting information

Supplementary data associated with this article can be found in the online version at doi:10.1016/j.triboint.2022.107509.

## References


[1] Ghaednia H, Wang X, Saha S, Xu Y, Sharma A, Jackson RL. A review of elastic-plastic contact mechanics. Appl Mech Rev 2017;69(6):060804–34.
[2] Persson BNJ. Contact mechanics for randomly rough surfaces. Surf Sci Rep 2006;61(4):201–27.
[3] Meng Y, Xu J, Jin Z, Prakash B, Hu Y. A review of recent advances in tribology. Friction 2020;8(2):221–300.
[4] DelRio FW, de Boer MP, Knapp JA, Reedy ED, Clews PJ, Dunn ML. The role of van der waals forces in adhesion of micromachined surfaces. Nat Mater 2005;4(8):629–34.
[5] Zhao YP, Wang LS, Yu TX. Mechanics of adhesion in mems–a review. J Adhes Sci Technol 2003;17(4):519–46.
[6] Greenwood JA, Williamson JBP. Contact of nominally flat surfaces. Proc R Soc A Math Phys Eng Sci 1966;295(1442):300–19.
[7] Whitehouse DJ, Archard JF. The properties of random surfaces of significance in their contact. Proc R Soc A Math Phys Eng Sci 1970;316(1524):97–121.
[8] Müser MH, Dapp WB, Bugnicourt R, Sainsot P, Lesaffre N, Lubrecht TA, et al. Meeting the contact-mechanics challenge. Tribol Lett 2017;65(118):1–18.
[9] Yastrebov VA, Anciaux G, Molinari JF. The role of the roughness spectral breadth in elastic contact of rough surfaces. J Mech Phys Solids 2017;107:469–93.
[10] Persson BNJ. On the fractal dimension of rough surfaces. Tribol Lett 2014;54(1):99–106.
[11] Bush AW, Gibson RD, Thomas TR. The elastic contact of a rough surface. Wear 1975;35(1):87–111.
[12] Polonsky IA, Keer LM. A numerical method for solving rough contact problems based on the multi-level multi-summation and conjugate gradient techniques. Wear 1999;231(2):206–19.
[13] Venugopalan SP, Nicola L, Müser MH. Green's function molecular dynamics: including finite heights, shear, and body fields. Modell Simul Mater Sci Eng 2017;25(3):034001.
[14] Murugesan Y, Venugopalan SP, Nicola L. On sub-surface stress caused by contact roughness in compressible elastic solids. Tribol Int 2021;159:106867.
[15] Johnson KL. Mechanics of adhesion. Tribol Int 1998;31(8):413–8.
[16] Tadmor EB, Ortiz M, Phillips R. Quasicontinuum analysis of defects in solids. Philos Mag A 1996;73(6):1529–63.
[17] Rudd RE, Broughton JQ. Concurrent coupling of length scales in solid state systems. Phys Status Solidi (b) 2000;217(1):251–91.
[18] Kohlhoff S, Gumbsch P, Fischmeister HF. Crack propagation in b.c.c. crystals studied with a combined finite-element and atomistic model. Philos Mag A 1991;64(4):851–78.
[19] Shilkrot LE, Miller RE, Curtin WA. Multiscale plasticity modeling: coupled atomistics and discrete dislocation mechanics. J Mech Phys Solids 2004;52(4):755–87.
[20] Dupuy LM, Tadmor EB, Miller RE, Phillips R. Finite-temperature quasicontinuum: molecular dynamics without all the atoms. Phys Rev Lett 2005;95:060202.
[21] Miller R, Ortiz M, Phillips R, Shenoy V, Tadmor EB. Quasicontinuum models of fracture and plasticity. Eng Fract Mech 1998;61(3):427–44.
[22] Pastewka L, Sharp TA, Robbins MO. Seamless elastic boundaries for atomistic calculations. Phys Rev B 2012;86:075459.
[23] Curtin WA, Miller RE. Atomistic/continuum coupling in computational materials science. Modell Simul Mater Sci Eng 2003;11(3):R33–68.
[24] Shabib I, Miller RE. A molecular dynamics study of twin width, grain size and temperature effects on the toughness of 2D-columnar nanotwinned copper. Modell Simul Mater Sci Eng 2009;17(5):055009.
[25] De Koning M, Kurtz RJ, Bulatov VV, Henager CH, Hoagland RG, Cai W, et al. Modeling of dislocation-grain boundary interactions in FCC metals. J Nuclear Mater 2003;323(2–3):281–9.
[26] Elzas A, Thijsse B. Dislocation impacts on iron/precipitate interfaces under shear loading. Modell Simul Mater Sci Eng 2016;24(8):085006.
[27] Aramfard M, Deng C. Mechanically enhanced grain boundary structural phase transformation in Cu. Acta Mater 2018;146:304–13.
[28] Elzas A, Thijsse B. Cohesive law describing crack growth at iron/precipitate interfaces. Comput Mater Sci 2017;134:214–24.
[29] Kastner O. Molecular-dynamics of a 2D model of the shape memory effect. Contin Mech Thermodyn 2013;15(5):487–502.
[30] Mani AZ, Jayadeep UB, Ramaseshan R. Molecular dynamics simulation of indentation on nanocoated surfaces: a comparison between 3D and 2D plane strain models. J Mater Res 2021;36(15):3063–73.
[31] Rafii-Tabar H, Hua L, Cross M. A multi-scale atomistic-continuum modelling of crack propagation in a two-dimensional macroscopic plate. J Phys Condens Matter 1998;10(11):2375–87.
[32] Brinckmann S, Mahajan DK, Hartmeier A. A scheme to combine molecular dynamics with dislocation dynamics. Modell Simul Mater Sci Eng 2012;20(4):045001.
[33] Henkelman G, Jónsson H. Improved tangent estimate in the nudged elastic band method for finding minimum energy paths and saddle points. J Chem Phys 2000;113(22):9978–85.
[34] Daw MS, Baskes MI. Embedded-atom method: derivation and application to impurities, surfaces, and other defects in metals. Phys Rev B 1984;29(12):6443.
[35] Mishin Y, Mehl MJ, Papaconstantopoulos DA, Voter AF, Kress JD. Structural stability and lattice defects in copper: Ab initio, tight-binding, and embedded-atom calculations. Phys Rev B 2001;63(22):224106.
[36] Lincoln RC, Koliwad KM, Ghate PB. Morse-potential evaluation of second-and third-order elastic constants of some cubic metals. Phys Rev 1967;157(3):463.
[37] Shenoy VB, Phillips R, Tadmor EB. Nucleation of dislocations beneath a plane strain indenter. J Mech Phys Solids 2000;48(4):649–73.
[38] Song J, Curtin WA, Bhandakkar TK, Gao HJ. Dislocation shielding and crack tip decohesion at the atomic scale. Acta Mater 2010;58(18):5933–40.
[39] Luan B, Robbins MO. Hybrid atomistic/continuum study of contact and friction between rough solids. Tribol Lett 2009;36(1):1–16.
[40] Nosé S. A unified formulation of the constant temperature molecular dynamics methods. J Chem Phys 1984;81(1):511–9.

[41] Hoover WG. Canonical dynamics: equilibrium phase-space distributions. Phys Rev A 1985;31(3):1695.
[42] Bitzek E, Koskinen P, Gähler F, Moseler M, Gumbsch P. Structural relaxation made simple. Phys Rev Lett 2006;97(17):170201.
[43] Thompson AP, Plimpton SJ, Mattson W. General formulation of pressure and stress tensor for arbitrary many-body interaction potentials under periodic boundary conditions. J Chem Phys 2009;131(15):154107.
[44] Tsuzuki H, Branicio PS, Rino JP. Structural characterization of deformed crystals by analysis of common atomic neighborhood. Comput Phys Commun 2007;177(6):518–23.
[45] Nyqvist J, Kadiric A, Ioannides S, Sayles R. Semi-analytical model for rough multilayered contacts. Trib Int 2015;87:98–112.
[46] Venugopalan SP, Nicola L, Müser MH. Green's function molecular dynamics: Including finite heights, shear, and body fields. Model Simul Mater Sci Eng 2017;25(3):34001.